Determining the electronic properties of semi-infinite crystals

Werner Hummel and H. Bross
Sektion Physik der Ludwig-Maximilians-Universität München, Theresienstraße 37, 80333 München, Germany
(Received 30 December 1996)

A self-consistent method for the calculation of the electronic structure of crystalline surfaces is described. It is based on a semi-infinite geometry with individual surface atomic layers stacked onto an infinite number of bulk layers. Contrary to models based on slab or superlattice geometries there is no artificial distortion of the correct asymptotic behavior of the wave functions so that an exact distinction between surface and bulk effects is possible. Furthermore there are no principal restrictions on the shape of the self-consistent potential. A special form of wave-function matching is used to construct the discrete surface states as well as the continuum of bulk states from complete sets of solutions of the Schrödinger equation in each single layer. The semi-infinite substrate is treated as a whole by means of the complex band structure which appears as an easily obtainable side-product of the theory. The main improvement at this step is the complete avoidance of the inherent numerical instability which prevented the application of similar matching techniques to other than very simple materials so far. The layer solutions of the Schrödinger equation are obtained by means of the spline-augmented-plane-wave method providing very accurate wave functions. As a first application the (001) and (111) surfaces of aluminum were investigated. The results obtained include the self-consistent charge density, the work function, and the complete band structure of the surface states and resonances. All calculations are found to be in good quantitative agreement with experiment. [S0163-1829(98)00124-6]

I. INTRODUCTION

For the theoretical investigation of the electronic structure of crystal surfaces within the framework of the local density approximation[1,2] (LDA), a variety of methods has been developed so far. According to their underlying model geometry they can be classified into two main groups. The first group to be mentioned here consists of the methods based on slab or superlattice geometries, where the influence of the bulk substrate is approximated by means of a finite number of interior atomic layers.[3–16] These models are of great popularity, arising from the fact that most of the well-approved techniques for calculating the band structure of a three-dimensional infinite crystal can be adapted without principal difficulties. Since the influence of the surface on the charge distribution is decaying within a few surface layers, these methods are well suited for the calculation of the charge density and related quantities. However, this is not the case for the investigation of eigenstates and other energy-resolved quantities which in general have a much greater spatial extension and are artificially modified in their decay behavior in such models. As a consequence an exact distinction between surface and bulk effects is lost. Moreover, the unavoidable interaction between the opposite surfaces leads to a splitting of all states which may reduce the energy resolution considerably. The consequences of these shortcomings may be diminished by increasing the number of layers, but the pay is an enormous increase of numerical expense.

These drawbacks do not arise with the other group of methods which are based on a semi-infinite geometry. Within this model, first self-consistent calculations were performed by Lang and Kohn on the assumption of a uniformly distributed charge background with some aspects of crystal structure taken into account perturbatively.[17,18] After that, a very general method of treating realistic semi-infinite crystals based on wave-function matching was proposed by Appelbaum and Hamann.[19,20] This approach, however, relied on the propagation matrix method[21,22] which was shown by Wachutka[23,24] to be not correct in the mathematical sense. In numerical calculations this mathematical deficit turns out as an inherent instability growing exponentially with the number of planar plane waves in the ansatz. For this reason, applications of that method to other than very simple materials were not successful so far.[25,26]

Other approaches followed[27–30] which were, however, not free of restrictions on the wave functions or the potential. Here, first self-consistent results were obtained by Inglesfield and Benesh[31] by means of the embedded potential method[28] applied to Al and Ni surfaces.

In order to avoid any of those restrictions, Wachutka returned to the ideas of Appelbaum an Hamann and showed how to replace the propagation matrix method to achieve mathematical correctness.[24] The main difference to the original approach was that the single layer problem was treated as a boundary value problem rather than as initial value problem.

In the present work these ideas are generalized, so that the problem connected to the boundary conditions vanishes completely. With the variations described below the approach of Appelbaum and Hamann now turns out as an efficient tool for the investigation of layered structures which combines the advantages of a semi-infinite geometry with high precision.

This treatment also saves a great amount of computer time, as the numerical effort is determined only by the relatively small number of atomic layers differing considerably from a bulk layer and, moreover, this expense increases only *linearly* with that number. This last feature makes the method particularly well suited for the investigation of materials with bad screening properties such as semiconductor

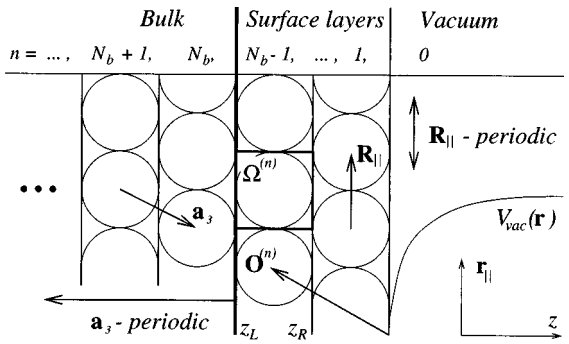

FIG. 1. Model of the semi-infinite crystal.

surfaces or heterostructures which require a greater number of individually treated layers than metals. Nevertheless, as a first application of the method the low indexed surfaces of aluminum are investigated.

II. SOLVING THE SCHRÖDINGER EQUATION

In order to obtain the solutions of the Schrödinger equation the semi-infinite crystal is divided into single atomic layers $z_L^{(n)} \leqslant z < z_R^{(n)}$ ($n=0,1,\ldots,\infty$; z denotes the coordinate perpendicular to the layers; $\mathbf{r}_\parallel$ the coordinates parallel to them) with the semi-infinite vacuum region considered as the zeroth layer (Fig. 1). Omitting reconstructions for the time being, all layers are invariant under translations by planar lattice vectors $\mathbf{R}_\parallel$. Since only a relatively small number of top layers are affected considerably by the surface, the assumption is made that all layers left from an appropriately chosen layer N_b (including that layer) already have the same effective potential V_{eff} and charge density ρ as the layer infinitely deep inside the crystal:

$$\phi_{\text{model}}^{(n)} = \begin{cases} \lim\limits_{k\to\infty} \phi^{(k)}, & n \geqslant N_b, \\ \phi^{(n)}, & n < N_b, \end{cases} \qquad \phi = V_{\text{eff}}, \rho. \tag{1}$$

In the following these identical layers are called bulk layers. It should be emphasized here, that in contrast to the potential the wave functions are not restricted in any way, but keep their correct asymptotic shape also deep inside the crystal. This is an important fact, because in general the effect of the surface on the wave functions has a much greater spatial extension than the effect on the potential or the charge density which are smoothened by screening effects and the integration over the Brillouin zone. Thus a much greater number of individually treated layers would be necessary—as in the case of slab based methods—if the wave functions were clipped too.

The solutions of the Schrödinger equation are now obtained by determining the total of partial solutions within each single layer followed by a matching procedure to give the differentiable global wave functions. Inside each single layer the Schrödinger equation is treated as a partial differential equation with the energy and the planar propagation vector $\mathbf{k}_\parallel$ considered as parameters. Because of the full three-dimensional periodicity of the potential inside the bulk region, the solutions within this domain can additionally be classified according to a third propagation vector component $k_\perp$ perpendicular to the surface. Since the bulk region is bounded at one side, this component may also be complex, thus leading to the concept of the complex band structure[32] which describes the total of solutions in this semi-infinite domain completely.

Up to this point the procedure essentially follows the ideas of Appelbaum and Hamann.[19] However, because of the inherent instability of the propagation matrix method used by these authors the further proceeding has to be altered.

A. The single layer problem

If $\mathcal{A}$ denotes the two-dimensional Wigner-Seitz cell of the planar periodic crystal with lattice vectors $\mathbf{R}_\parallel$, then a single layer is represented by an elementary region $\Omega = \mathcal{A}\times[z_L, z_R[$ and the problem is to find all solutions of the Schrödinger equation within this layer with the Bloch property

$$\psi_{\mathbf{k}_\parallel E}(\mathbf{r}_\parallel + \mathbf{R}_\parallel, z) = e^{i\mathbf{k}_\parallel\cdot\mathbf{R}_\parallel}\psi_{\mathbf{k}_\parallel E}(\mathbf{r}_\parallel, z) \tag{2}$$

for a given planar propagation vector $\mathbf{k}_\parallel$ and energy E. However, since the application of a variational principle requires the problem stated to have a unique solution, a further boundary condition has to be imposed. In the case of the propagation (or transfer-[22,33,34]) matrix method this additional condition is the specification of the value and the normal derivative of ψ at *one* side of the layer. This works well with one-dimensional, i.e., ordinary differential equations, but it fails when applied to a partial (elliptic) differential equation. To state this problem correctly, the boundary conditions must be enclosing, i.e., imposed on *both* sides.[23,24,35] A proper choice are Dirichlet boundary conditions, where the value of ψ is specified on the whole boundary and the normal derivative is left free. Since the Bloch property (2) can be shown to work as a correct ''enclosing'' boundary condition in the parallel directions,[23] we are left with the condition

$$\psi_{\mathbf{k}_\parallel}(\mathbf{r}_\parallel, z_X) = \sum_{\mathbf{K}_\parallel} b_{\mathbf{K}_\parallel}^X e^{i(\mathbf{k}_\parallel+\mathbf{K}_\parallel)\mathbf{r}_\parallel} \quad \text{for} \quad X \in \{L,R\}, \tag{3}$$

where $\underline{b}^X$ are the Fourier coefficients of an arbitrary Bloch periodic function defined on the layer boundaries X. $\mathbf{K}_\parallel$ denotes the two-dimensional reciprocal lattice vectors. Now, there exists a unique and stable solution for any given values of $\underline{b}^X$, exactly if there is no nontrivial solution which vanishes at both sides of the layer. However, such solutions with a boundary value of zero only exist at discrete energies (for fixed $\mathbf{k}_\parallel$) which are equal to the energy eigenvalues of the layer enclosed in an infinitely deep well. Because these energies constitute a set with measure zero they can be neglected in connection with energy-integrated (physical) quantities such as the charge density, but they may cause numerical effects when calculating the wave function which are discussed later.

For wave functions ψ satisfying Eqs. (2) and (3), it is easy to show that the Schrödinger equation is equivalent to the variational problem

$$\delta\Phi(\psi,\psi) = 0 \quad \text{for given} \quad \underline{b}^X, \tag{4}$$

where

$$\Phi(\xi,\psi) := H(\xi,\psi) - ES(\xi,\psi) \tag{5}$$

and

$$S(\xi,\psi):=\int_\Omega \xi(\mathbf{r})^*\psi(\mathbf{r})d^3\mathbf{r},$$

$$H(\xi,\psi):=\int_\Omega \{[\nabla\xi(\mathbf{r})^*][\nabla\psi(\mathbf{r})]+V_{\text{eff}}(\mathbf{r})\xi(\mathbf{r})^*\psi(\mathbf{r})\}\ d^3\mathbf{r} \tag{6}$$

in atomic units with $\hbar=1$, $m_e=\frac{1}{2}$, and $e^2=2$. Thus, the whole set of solutions within the layer is obtained by solving Eq. (4) for wave functions ψ subjected to all possible boundary values $\underline{b}^X$.

In the case of crystal layers this is done by means of a spline-augmented-plane-wave (SAPW) ansatz, adapted to layer structure. This ansatz, standing out for high precision results in bulk calculations,[36] combines several advantages with regard to the layer problem too.

For $\mathbf{r}\in\Omega$ and—for the sake of simplicity—one atom per elementary region (the location of which defines the layer origin), this ansatz reads

$$\psi_{\mathbf{k}_\parallel}(\mathbf{r})=\sum_{\mathbf{K}_\parallel}^{N_k}\sum_{\lambda} A_{\mathbf{K}_\parallel\lambda}S_\lambda(z)e^{i(\mathbf{k}_\parallel+\mathbf{K}_\parallel)\mathbf{r}_\parallel}+\Theta(r_{\text{MT}}-r)$$
$$\times\sum_{l,m}^{l_{\max}}\sum_{\rho} B_{lm\rho}i^{|m|}r^l R_\rho^l(r)Y_{lm}(\mathbf{r}_0)=\sum_i C_i\varphi_i(\mathbf{r}). \tag{7}$$

It consists of an expansion in planar reciprocal lattice vectors with z-dependent coefficients which is augmented by a multipole expansion within a muffin-tin (MT) sphere to approximate the strong oscillations of the wave function in the vicinity of the nucleus. All sums are finite. The z-dependent planar Fourier coefficients are represented as sums over a λ-indexed system of ansatz functions $S_\lambda(z)$ with coefficients $A_{\mathbf{K}_\parallel\lambda}$. The MT sphere with radius r_{MT} is inscribed into Ω. The Y_{lm} are real spherical harmonics. Together with the factor $i^{|m|}$ they allow a real valued calculation for lattices with (two-dimensional) inversion symmetry. The $R_\rho^l(r)$ are a ρ-indexed system of radial ansatz functions, independent of energy or the propagation vector. The factor r^l ensures proper behavior at the origin. N_k denotes the number of planar reciprocal lattice vectors and $l_{\max}$ the maximum value of l in the ansatz. Finally, φ_i and C_i are a condensed notation of the ansatz functions and their coefficients, respectively.

The wave functions are differentiable due to the condition

$$R_\rho^l(r)=\frac{d}{dr}R_\rho^l(r)=0 \quad \text{for} \quad r\geqslant r_{\text{MT}}. \tag{8}$$

In order to achieve good approximation properties and to facilitate the dealing with the boundary conditions (8) and (3) we use cubic B-splines for the functions $R_\rho^l(r)$ as well as for $S_\lambda(z)$.

In general, for a given interval $[x_L,x_R[$, such a system is defined on a partition $\{x_L=x_0<x_1<\cdots<x_N=x_R\}$ as a set of piecewise cubic polynomials:

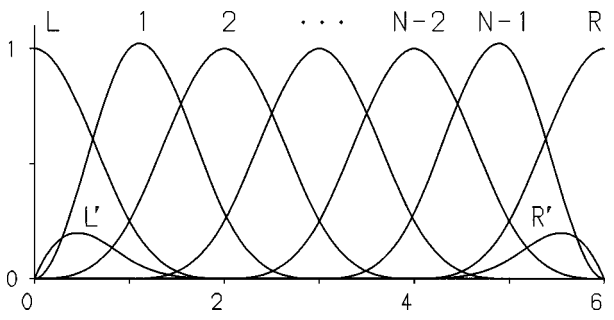

FIG. 2. B-spline system for $N=6$ with break points $x_j=j$.

$$B_\lambda(x)=\sum_{j=0}^{N-1}\chi_j(x)\sum_{k=0}^{3}B_{\lambda jk}(x-x_j)^k,$$

$$\chi_j(x):=\begin{cases}1 & x\in[x_j,x_{j+1}[,\\ 0 & \text{otherwise.}\end{cases} \tag{9}$$

They must be twice differentiable and nonzero only on at most four partition intervals.[36,37] The last property later results in matrices of band form. For the indices $\lambda\in\{1,\ldots,N-1,L,R,L',R'\}$ these systems are uniquely determined by the requirement of having a minimal supplement and the conditions (see Fig. 2)

$$B_\lambda(x_X)=\delta_{\lambda X},\quad X=L,R,$$

$$B'_\lambda(x_L)=\delta_{\lambda L'},\quad B'_\lambda(x_R)=-\delta_{\lambda R'},$$

$$B_\lambda(x_\lambda)=1,\quad \lambda=1,\ldots,N-1. \tag{10}$$

According to this notation, the indices L and R denote these two splines which have nonvanishing values but zero derivatives at the boundaries of the interval $[x_L,x_R[$, while L' and R' denote those two splines which have nonvanishing derivatives but zero values at the boundaries. All other splines have both vanishing values and vanishing derivatives at the boundaries.

In that manner the spline systems S_λ and R_ρ^l are defined on the intervals $[z_L,z_R[$ and $[0,r_{\text{MT}}[$, respectively, with the break points

$$z_j=z_L+(z_R-z_L)j/N_z,\quad j=0,\ldots,N_z,$$

$$r_{lj}=r_{\text{MT}}(j/N_r^l)^2,\quad j=0,\ldots,N_r^l; \tag{11}$$

l dependent in the latter case, to account for the different oscillation strengths of the different multipole components.

According to Eq. (10), the condition (8) is now ensured by omitting the values R and R' in the index ρ. Since the MT sphere is inscribed in Ω there is no contribution of the radial functions to the boundary values of the layer which are simply given by

$$b^X_{\mathbf{K}_\parallel}=A_{\mathbf{K}_\parallel X}, \tag{12}$$

and the condition (3) can easily be fulfilled by fixing these coefficients. Variation of the other coefficients then leads to a *homogeneous underdetermined* system of linear equations

$$\sum_i \Phi(\varphi_{\hat{j}},\varphi_i)C_i=0 \quad \text{for} \quad \hat{j}\neq(\mathbf{K}_\parallel,X), \quad X\in\{L,R\}, \tag{13}$$

which has a $2N_k$-dimensional solution space corresponding to the space of possible boundary values $\underline{b}^X$ and therefore to the whole set of layer solutions of the Schrödinger equation within the given ansatz.

Because of the division of the whole crystal in layers treated quite independently, the numerical effort of our method increases only linearly with the number of surface layers. It is essential for this linearity that the above systems of equations are independent for each layer. This requires the MT spheres to lie completely within their respective layer. However, for high index faces the MT radius will become very small requiring the plane wave part of the ansatz to increase in order to describe the wave function accurately. This turns out to be tolerable for (001), (111), or (011) faces, where the considerable reduction of numerical effort due to the above-mentioned linearity predominates, but may become a problem for higher index faces.

A possible solution is to keep large MT spheres and to cut off the segments jutting out over the layer boundaries. These segments are then turned back into their own layer to take the place of the penetrating segments of the MT spheres of other layers. In this case the plane wave part of the ansatz has to approximate only the difference of segments of the radial functions of adjacent layers which requires considerably less plane waves than an accurate approximation of segments of the radial functions themselves. However, the matching procedure of the wave function of adjacent layers becomes more complicated since the radial functions now contribute to the boundary values, too. Furthermore, it is generally no longer possible to fulfill the matching conditions exactly. Thus, instead of solving an exact matching equation, we have to perform a least squares fit of the boundary values (and derivatives) of adjacent layers. However, since this procedure also results in a system of linear equations [similar to Eq. (20)], we do not have to change our overall proceeding in this case.

In the vacuum region the potential behaves rather smoothly, thus a simple planar Fourier ansatz is sufficient. Since the deviation of the potential from its asymptotic level $V(z\to\infty)\equiv 0$ becomes very small in a short distance from the surface, we can neglect the difference on the right of an appropriate chosen boundary z_R^{vac} and assume the potential to be exactly equal to the asymptotic level for $z\geqslant z_R^{\mathrm{vac}}$. In this case the exact solutions for $z\geqslant z_R^{\mathrm{vac}}$ are given by exponentials. In the vicinity of the surface ($z_L^{\mathrm{vac}}\leqslant z<z_R^{\mathrm{vac}}$) the greater deviations from the asymptotic shape are taken into account by superposing a B-spline system. Hence, the vacuum ansatz reads

$$\psi_{\mathbf{k}_\parallel}^{\mathrm{vac}}(r)=\sum_{\mathbf{K}_\parallel}^{N_k}\sum_{\lambda\neq R'} C_{\mathbf{K}_\parallel\lambda}\hat{S}_\lambda^{\mathrm{vac}}(z)e^{-\kappa_{\mathbf{K}_\parallel}z}e^{i(\mathbf{k}_\parallel+\mathbf{K}_\parallel)\mathbf{r}_\parallel}, \tag{14}$$

with $\kappa_{\mathbf{K}_\parallel}:=\sqrt{(\mathbf{k}_\parallel+\mathbf{K}_\parallel)^2-E}$. The spline system is defined on quadratically spaced break points $z_j^{\mathrm{vac}}=z_L^{\mathrm{vac}}+(z_R^{\mathrm{vac}}-z_L^{\mathrm{vac}})(j/N_{\mathrm{vac}})^2$, $j=0,\ldots,N_{\mathrm{vac}}$ and is continued constantly for $z>z_R^{\mathrm{vac}}$ according to $\hat{S}_\lambda^{\mathrm{vac}}(z>z_R^{\mathrm{vac}})=\hat{S}_\lambda^{\mathrm{vac}}(z_R^{\mathrm{vac}})$ (which is nonzero only for $\lambda=R$). In order to maintain differentability at z_R^{vac} the index $\lambda=R'$ must be excluded in Eq. (14).

Since in the vacuum region only the left boundary values $b_{\mathbf{K}_\parallel}^L=C_{\mathbf{K}_\parallel L}$ can be chosen arbitrarily, the resulting underdetermined linear system

$$\sum_i \Phi(\varphi_j^{\mathrm{vac}},\varphi_i^{\mathrm{vac}})C_i=0 \quad \text{for} \quad \hat{j}\neq(\mathbf{K}_\parallel,L), \tag{15}$$

has only an N_k-dimensional space of solutions.

The obvious way to solve the underdetermined linear systems (13) and (15) is to separate the part of the coefficients belonging to the boundary values $\underline{b}^X$ together with the respective columns of the matrix $\Phi(\varphi_i,\varphi_j)$ and put it on the right-hand side of the equation, leaving a quadratic matrix on the left side. This can be solved as a regular linear system for all values of $\underline{b}^X$. This works well in almost all cases. However, for energies close to the abovementioned values for which there exist solutions with a boundary value of zero the matrix on the left-hand side becomes almost singular. So, following the simplest way leads to some numerical trouble even in the case of a mathematically properly stated Dirichlet problem.

However, these problems can be completely avoided, if the special treatment of the boundary values is abandoned—as already suggested by the representation as an underdetermined system—and an arbitrary parametrization of the solution space is permitted. In this case, the actual choice of columns of Φ to be put on the right hand side, can be left to numerical standard procedures which leave an optimally conditioned matrix on the left hand side. For this purpose we used a QR-factorization algorithm for rectangular matrices as described in well-established numerical libraries combined with a partial pivot search. Solving the linear systems for all right-hand sides selected in this manner now gives an optimal set of basis vectors of the solution spaces for *all* energies. If these basis vectors are put together columnwise in the matrix G, the coefficients of the general solution are given—numerically stable—by

$$\underline{C}=G\underline{\beta}, \quad \underline{\beta}\in\mathcal{C}^{N_xN_k} \tag{16}$$

with a generalized parametrization $\underline{\beta}$. Here, N_x denotes the number of layer boundaries with variable boundary conditions, i.e., $N_x=1$ in the vacuum layer and $N_x=2$ in all other layers.

B. The matching procedure

The quantities to be considered in the matching procedure are the vector of the Fourier coefficients of the boundary values $\underline{b}^X\in\mathcal{C}^{N_k}$ and the vector $\underline{b}'^X$ defined by

$$\frac{\partial}{\partial z}\psi_{\mathbf{k}_\parallel}(\mathbf{r}_\parallel,z_X)=\sum_{\mathbf{K}_\parallel} b'^X_{\mathbf{K}_\parallel}e^{i(\mathbf{k}_\parallel+\mathbf{K}_\parallel)\mathbf{r}_\parallel}, \tag{17}$$

describing the normal derivatives. They are obtained from the coefficients $\underline{C}$ by multiplication with simple projection matrices P_X determined by relations such as Eq. (12). Hence, the boundary values and derivatives of the general solution of the Schrödinger equation within a layer can be written as

$$\begin{pmatrix} \underline{b}^X \\ \underline{b}'^X \end{pmatrix} =: P_X \underline{C} = \Pi_X \underline{\beta} \tag{18}$$

with $\Pi_X := P_X G \in \mathcal{C}^{2N_k \times N_x N_k}$.

For convenience each single layer is supplied with its own coordinate system, the origins of which are denoted by the vectors $\mathbf{O}^{(n)}$. Thus, the matching condition for the solutions of adjacent layers takes the form

$$\begin{pmatrix} \psi^{(n+1)} \\ \partial_z \psi^{(n+1)} \end{pmatrix}_{(\mathbf{r}_\parallel + \mathbf{O}_\parallel^{(n)} - \mathbf{O}_\parallel^{(n+1)},\, z_R^{(n+1)})} = \begin{pmatrix} \psi^{(n)} \\ \partial_z \psi^{(n)} \end{pmatrix}_{(\mathbf{r}_\parallel, z_L^{(n)})} . \tag{19}$$

This leads to a underdetermined linear system of equations for the coefficients $\underline{\beta}$ of adjacent layers:

$$t_\parallel^{(n)} T_2^{(n)} \Pi_R^{(n+1)} \underline{\beta}^{(n+1)} = \Pi_L^{(n)} \underline{\beta}^{(n)}, \tag{20}$$

where

$$t_\parallel^{(n)} := e^{i\mathbf{k}_\parallel (\mathbf{O}_\parallel^{(n)} - \mathbf{O}_\parallel^{(n+1)})} \tag{21}$$

and

$$T_2^{(n)} := \begin{pmatrix} T^{(n)} & 0 \\ 0 & T^{(n)} \end{pmatrix} \quad \text{with} \quad T^{(n)} := \mathrm{diag}_{\mathbf{K}_\parallel} \{ e^{i\mathbf{K}_\parallel (\mathbf{O}_\parallel^{(n)} - \mathbf{O}_\parallel^{(n+1)})} \}. \tag{22}$$

The notation $\mathrm{diag}_i A(i)$ with a quantity $A(i)$ stands for the diagonal matrix with diagonal elements $A(i)$.

Within the bulk we can take advantage of the additional periodicity in the third direction described by the vector $\mathbf{a}_3 = \mathbf{O}^{(n)} - \mathbf{O}^{(n+1)}$, $n \geqslant N_b$ which allows the classification of the solutions in this region according to a third Bloch vector component $k_\perp$:

$$\psi_{\mathbf{k}_\parallel k_\perp} (\mathbf{r}_\parallel + \mathbf{a}_{3\parallel}, z + a_{3\perp}) = e^{i\mathbf{k}_\parallel \mathbf{a}_{3\parallel}} e^{ik_\perp a_{3\perp}} \psi_{\mathbf{k}_\parallel k_\perp} (\mathbf{r}_\parallel, z). \tag{23}$$

In contrast to the infinitely extended crystal, the range of values to be taken into account for $k_\perp$ also includes the lower complex plane in the case of the semi-infinite bulk. Since the exponential increase of such wavefunctions in the z direction is cut at the bulk boundary, those wave functions remain normalizable with respect to the semi-infinite bulk and may therefore contribute to global physical solutions. Thus, the whole set of solutions within the bulk is described completely (only) by the complex band structure.[32]

The condition (23) is equivalent to a boundary condition posed onto one representative bulk layer

$$\begin{pmatrix} \psi_{\mathbf{k}_\parallel k_\perp} \\ \partial_z \psi_{\mathbf{k}_\parallel k_\perp} \end{pmatrix}_{(\mathbf{r}_\parallel + \mathbf{a}_{3\parallel}, z_R)} = t_\perp t_\parallel \begin{pmatrix} \psi_{\mathbf{k}_\parallel k_\perp} \\ \partial_z \psi_{\mathbf{k}_\parallel k_\perp} \end{pmatrix}_{(r_\parallel, z_L)} . \tag{24}$$

Here $t_\parallel$ and T_2 are given by Eq. (22) for $n \geqslant N_b$ in which case these definitions become independent of n, and $t_\perp := e^{ik_\perp a_{3\perp}}$.

This leads to a $2N_k$-dimensional general non-Hermitian eigenvalue problem

$$T_2 \Pi_R \underline{\beta} = t_\perp \Pi_L \underline{\beta} \tag{25}$$

providing the—with respect to the ansatz—complete complex band structure $k_\perp^\mu(\mathbf{k}_\parallel, E)$ and the corresponding eigenvectors $\underline{\beta}^\mu(\mathbf{k}_\parallel, E)$, $\mu = 1, \ldots, 2N_k$ for given E and $\mathbf{k}_\parallel$.

Here, the real eigenvalues $k_\perp$ correspond to propagating wave functions and therefore to the usual band structure of the infinite crystal. Because of the periodicity of the inverse function $E(k_\perp)$ along the real axis the number of real $k_\perp$ for given E is—except for discrete energies—always even and is denoted by $2\sigma_p$, $\sigma_p \in \mathcal{N}_0$ in the following. The eigenvalues with $\mathrm{Im}\, k_\perp < 0$ correspond to the so called *evanescent waves* which are normalizable in contrast to their infinitely increasing counterparts with $\mathrm{Im}\, k_\perp > 0$. Because of the three-dimensional inversion symmetry of a bulk layer and time reversal invariance there are as many eigenvalues on the upper as on the lower complex plane, so their number equals $N_k - \sigma_p$.

Thus, the whole set of physically relevant solutions within the bulk is described by the matrix

$$B^{(N_b)} \equiv (\overbrace{B_p}^{2\sigma_p}, \overbrace{B_e}^{N_k - \sigma_p}) \quad \in \mathcal{C}^{2N_k \times (N_k + \sigma_p)} \tag{26}$$

where the columns of B_p are the $2\sigma_p$ eigenvectors $\underline{\beta}^\mu$ corresponding to propagating solutions with $k_\perp^\mu \in \mathcal{R}$ and B_e consists of the eigenvectors corresponding to the evanescent waves with $\mathrm{Im}\, k_\perp < 0$.

Starting from the general solution within the bulk which can be parametrized according to

$$\underline{\beta}^{(N_b)} = B^{(N_b)} \underline{\alpha}^{(N_b)}, \ \alpha^{(N_b)} \in \mathcal{C}^{N_k + \sigma_p} \tag{27}$$

by means of a $(N_k + \sigma_p)$-dimensional vector $\underline{\alpha}^{(N_b)}$, we can now match the $(N_b - 1)$th layer via Eq. (20) to the bulk and have again a $(N_k + \sigma_p)$-dimensional solution space. This can in turn be parametrized by a vector $\underline{\alpha}^{(N_b - 1)}$. This procedure can be continued up to the vacuum layer and leads to an iterative linear system of homogeneous underdetermined equations for the construction of the overall solution

$$\left(\overbrace{t_\parallel^{(n)} T_2^{(n)} \Pi_R^{(n+1)} B^{(n+1)}}^{N_k + \sigma_p}, \overbrace{-\Pi_L^{(n)}}^{N_x^{(n)} N_k} \right) \begin{pmatrix} \underline{\alpha}^{(n+1)} \\ \underline{\beta}^{(n)} \end{pmatrix} = \underline{0} \quad \in \mathcal{C}^{2N_k} \tag{28}$$

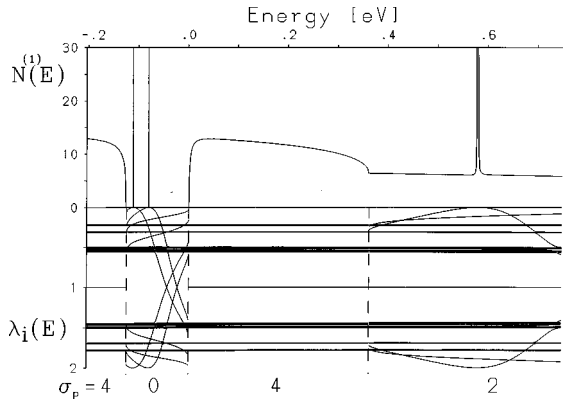

FIG. 3. Mismatch eigenvalues $\lambda_i(E)$ of Eq. (36) and surface density of states (39) of Al(001) for $\mathbf{k}_\parallel=(28M+X)/29$ (a.u.) with $N_k=24$. There are two surface states in the band gap around -0.1 eV and a sharp surface resonance at 0.58 eV. The eigenvalues are symmetric with respect to 1. Most of them are almost constant and accumulate in the broadened horizontal lines.

which has to be solved for $n=N_b-1,\ldots,0$. Obviously the numerical effort increases only linearly with the number of surface layers N_b. As in the case of Eq. (13) the stability of the numerical solution of Eq. (28) can be guaranteed by standard procedures. The basis vectors of the solution space of the nth equation are put together columnwise to form a matrix $\binom{A^{(n+1)}}{B^{(n)}}$ which defines the matrix $B^{(n)}$ for the next equation. The coefficients

$$\underline{\alpha}^{(n)} \in \begin{cases} \mathcal{C}^{N_k+\sigma_p} & \text{for } n>0, \\ \mathcal{C}^{\sigma_p} & \text{for } n=0, \end{cases} \tag{29}$$

then parametrize the solutions of Eq. (28) according to

$$\begin{matrix} N_{k+\sigma_p} \\ N_x^{(n)} N_k \end{matrix} \left\{ \begin{matrix} \\ \\ \end{matrix} \right. \begin{pmatrix} \underline{\alpha}^{(n+1)} \\ \underline{\beta}^{(n)} \end{pmatrix} =: \begin{pmatrix} A^{(n+1)} \\ B^{(n)} \end{pmatrix} \underline{\alpha}^{(n)}. \tag{30}$$

After solving the complete system, only the coefficient vector $\underline{\alpha}^{(0)} \in \mathcal{C}^{\sigma_p}$ remains undetermined and parametrizes finally a σ_p-dimensional space of overall solutions $\psi_{\mathbf{k}_\parallel E_j}$, $j=1,\ldots,\sigma_p(\mathbf{k}_\parallel E)$. Thus, we obtain the familiar fact that one surface adapted state exists for every two propagating bulk solutions. Within the bulk bands this results in a continuum of surface adapted bulk states, the so-called projected band structure for fixed $\mathbf{k}_\parallel$. Within the bulk bandgaps, on the other hand, σ_p is zero and the last equation (28) for $n=0$ is regular, so that there exist nontrivial solutions—the pure surface states—at most at discrete energies E_i^s. Therefore, we have an unambiguous distinction between surface and bulk states in a natural way. A major shortcoming of slab based methods is the lack of this criterion.

The states within the continuum are normalized according to

$$\int_{\mathcal{R}^3} \psi^{p*}_{\mathbf{k}'_\parallel E' j'} \psi^{p}_{\mathbf{k}_\parallel E j}\, d^3\mathbf{r} = \delta^2(\mathbf{k}'_\parallel-\mathbf{k}_\parallel)\,\delta(E'-E)\,\delta_{j'j},$$

$$j,j'=1,\ldots,\sigma_p, \tag{31}$$

(current normalization) and discrete surface states according to

$$\int_{\mathcal{R}^3} \psi^{s*}_{\mathbf{k}'_\parallel E^s_i, j'} \psi^{s}_{\mathbf{k}_\parallel E^s_i j}\, d^3\mathbf{r} = \delta^2(\mathbf{k}'_\parallel-\mathbf{k}_\parallel)\,\delta_{i'i}\delta_{j'j},$$

$$j,j'=1,\ldots,\sigma_s, \tag{32}$$

where σ_s denotes the degree of degeneracy of the latter.

Finding surface states and resonances. The discrete energies of the surface states can be found reliably by looking at the residue on the right-hand side of Eq. (28) for $n=0$, i.e., the mismatch between the surface and the vacuum:

$$\underline{\Delta b} := t_\parallel^{(0)} T_2^{(0)} \begin{pmatrix} \underline{b}^R \\ \underline{b}'^R \end{pmatrix}^{(1)} - \begin{pmatrix} \underline{b}^L \\ \underline{b}'^L \end{pmatrix}^{(0)} = F\underline{x}, \tag{33}$$

where $F := (t_\parallel^{(0)} T_2^{(0)} \Pi_R^{(1)} B^{(1)}, -\Pi_L^{(0)})$, $\underline{x} := \binom{\underline{\alpha}^{(1)}}{\underline{\beta}^{(0)}}$. With the normalizing condition

$$\left\| \begin{pmatrix} \underline{b}^R \\ \underline{b}'^R \end{pmatrix}^{(1)} \right\|^2 + \left\| \begin{pmatrix} \underline{b}^L \\ \underline{b}'^L \end{pmatrix}^{(0)} \right\|^2 =: \underline{x}^\dagger M \underline{x} \overset{!}{=} 1, \tag{34}$$

where M is determined by the definitions (18) and (30), we obtain a measure of the mismatch which is independent of the particular parametrization of the various solution spaces:

$$\Delta(E) := \min_{\underline{x}^\dagger M \underline{x}=1} \|\underline{\Delta b}\|^2. \tag{35}$$

With this, the energy eigenvalues of the surface states are determined by $\Delta(E)=0$. The minimization of $\|\underline{\Delta b}\|^2$ leads to a general hermitian eigenvalue problem

$$(F^\dagger F - \lambda M)\underline{x} = 0, \tag{36}$$

with eigenvalues λ_i which are the extremum values of $\|\underline{\Delta b}\|^2$ under the condition (34). Moreover, the corresponding mismatch vectors fulfil the orthogonality relation

$$\underline{\Delta b}_i^\dagger \cdot \underline{\Delta b}_j = \lambda_i \delta_{ij}. \tag{37}$$

Hence, Δ is given by the smallest eigenvalue $\lambda_{\min}$.

As is demonstrated by Fig. 3 the best way to find the zeros of $\Delta(E)$ is to obverve the course of all eigenvalues λ_i separately. Since the eigenvalues turn out to be smooth functions of E, their zeros can be detected without problems by numerical standard methods. The correct assigning of the eigenvalues at different energies can be performed by means of Eq. (37) which is approximately valid also for slightly different energies of $\underline{\Delta b}_i$ and $\underline{\Delta b}_j$. The essential advantage of this procedure is, that in the case of degenerate or almost degenerate surface states, these states are—for orthogonality reasons—indicated by different eigenvectors of Eq. (36), so there is no risk of overlooking one of them.

The method described above is also applicable to the detection of surface resonances—narrow peaks of the surface density of states within the continuum of bulk states (where $\sigma_p>0$)—which turns out below to be a critical point in the calculation of the charge density. An appropriate measure for the distinction of a surface resonance is obviously the smallness of the contribution of propagating waves in the bulk. Therefore, if we temporarily omit these propagating bulk solutions, we expect the residue in Eq. (28) or Δ to have a

minimum at the point of a resonance which allows its reliable detection as above. Of course, the propagating waves are only omitted for the purpose of finding the resonances. After their detection the propagating solutions are fully taken into account again.

The propagating waves can simply be excluded by inserting the matrix $B_e^{(N_b)}$ of Eq. (26) instead of $B^{(N_b)}$ into Eq. (28). Since its solution space then loses $2\sigma_p$ dimensions, an iterative definition of matrices $B_e^{(n)}$ for $n<N_b$ in analogy to Eq. (30) and their insertion into Eq. (28) are consistent. Proceeding in this manner we are left with an overestimated equation for $n=0$, the nonvanishing residue of which can be treated as in the case of surface states. The corresponding eigenvalues of Eq. (36) are shown in Figure 3 too. This picture also demonstrates that—in contrast to the eigenvalues—the surface density of states is not an appropriate means to detect surface resonances. Unless the energy range is scanned in very small, time consuming steps (here some meV) there is only a small chance to encounter an indication of the extremely narrow peak of the surface density of states by looking only at the surface density of states.

III. CHARGE DENSITY AND EFFECTIVE POTENTIAL

The $\mathbf{k}_\parallel$-resolved local density of states $n(\mathbf{k}_\parallel,E,\mathbf{r})$ is given by the contributions of the normalized bulk and surface states ψ^p and ψ^s, respectively, as

$$n(\mathbf{k}_\parallel,E,\mathbf{r})=\sum_{j=1}^{\sigma_p}|\psi^p_{\mathbf{k}_\parallel Ej}(\mathbf{r})|^2 + \sum_i \delta[E-E_i^s(\mathbf{k}_\parallel)]\sum_{j=1}^{\sigma_s}|\psi^s_{\mathbf{k}_\parallel Ej}(\mathbf{r})|^2. \quad (38)$$

The layer density of states (LDOS) is then defined by

$$N^{(n)}(\mathbf{k}_\parallel,E):=\int_{\Omega^{(n)}} n(\mathbf{k}_\parallel,E,\mathbf{r})\; d^3\mathbf{r}, \quad (39)$$

and the charge density ρ is obtained as usual by integration over the occupied states

$$\rho(\mathbf{r})=\frac{2A_\parallel}{(2\pi)^2}\int_{BZ_2}\int_{-\infty}^{E_F} n(\mathbf{k}_\parallel,E,\mathbf{r})\; dE\,d^2\mathbf{k}_\parallel. \quad (40)$$

Here the Fermi energy E_F is determined implicitly by the requirement of charge neutrality for the whole crystal. However, because of their predominance only the (infinitely remote) bulk layers do contribute to this term. This leads to the following neutrality condition:

$$\lim_{n\to\infty}\int_{\Omega^{(n)}}\rho(\mathbf{r})\; d^3\mathbf{r}=\frac{2V_\Omega}{(2\pi)^3}\times\int_{BZ_2}\int_{-\infty}^{E_F}\sum_{\mu=1}^{2\sigma_p}\left|\frac{\partial k_\perp^\mu}{\partial E}\right| dE\,d^2\mathbf{k}_\parallel \overset{!}{=} Z_{\mathrm{nuc}}^{(b)}, \quad (41)$$

where the second expression is obtained from the first, after some calculation, taking into account the asymptotic behavior of the wave functions inside the bulk. Since $|\partial_E k_\perp^\mu|$ is just the Jacobian determinant of the transformation $k_\perp^\mu\to E$, the above condition is—as expected—equivalent to the corresponding relation for the infinite crystal. As the equation (and therefore the Fermi energy, too) only depends on pure bulk properties there is no *a priori* constraint on the charges in the surface layers, so these quantities are free to be determined in the course of the self-consistency procedure.

The $\mathbf{k}_\parallel$ integrations in the above expressions are performed in the usual manner by summing over an irreducible grid of special points[38,39] specified, e.g., by Cunningham.[40] In the case of Al(001) and Al(111) a number of ten and eight points, respectively, proved to be sufficient. However, the energy integration which has to be executed before, turns out to be not so simple because of some unpleasant properties of the integrand. The first problem to cope with arises from the van Hove singularities appearing at the edges E_e of the real bulk bands (where σ_p changes its value). For fixed $\mathbf{k}_\parallel$ these singularities behave as $|E-E_e|^{+1/2}$ in layers in finite distance from the surface and as $|E-E_e|^{-1/2}$ in the infinite remote bulk layer.[41] They can be integrated accurately after the substitution $E\to t=|E-E_e|^{1/2}$ of the integration variable which transforms these singularities into polynomials. However, before this is possible, one actually has to find all of those edge points what turns out to be the main problem, particularly in the case of narrow bands. To overcome this difficulty, a method based on the pursuit of the curvature of the complex band structure proved to be very reliable. Because the real band edges are exactly the points where the complex bands branch off,[32] one has to search for the zeros of $\mathrm{Im}\,k_\perp$ in that case. The advantage of looking at the complex bands lies in the fact that all of these lines—even if connected with the narrowest real bands—are extended over the whole energy range for complex $k_\perp$,[32] thus indicating each crossing with the real axis in a distance sufficient to be detected by standard algorithms.

Nevertheless, in the case of the very narrow core bands this expense would not be reasonable. Because the corresponding charge density is only slightly affected by the presence of the surface, it is favorable to take this part of the density from a separate (self-consistent) bulk calculation and freeze it during the self-consistency procedure for the surface. In case of aluminum, the two lowest core states can be treated in that manner with a relative error of less than one percent.

The other problem connected to the energy integration is due to the surface resonances, the peaks of which often show an extremely small width, typically in the range of 1/100 eV and below (also see Fig. 3). By applying usual integration grids these peaks either remain undetected or—the worse case—accidentially run into a grid point and add a considerable random contribution to the charge density destroying any possible convergence of the self-consistency procedure. In the present approach this problem is remedied, somewhat coarsely, by simply inserting a sufficient number of additional grid points into small intervals around each resonance peak which can be localized reliably by scanning the smoothly varying eigenvalues in Eq. (36) as described before.

With the exceptions mentioned above, the integrand behaves rather smoothly, so that no loss of precision is expected with further integration. In the case of aluminum, a

total number of 80 energy grid points proved to be sufficient to achieve an accuracy of three digits.

A more elegant way of performing the energy integration would be to take advantage of the analytic properties of the density of states and to integrate instead over a contour in the complex energy plane where the integrand varies only smoothly. However, the handling of complex energies which appears quite natural in a formalism based on Green's functions would require more elaborate investigations in the present approach.

As a consequence of the mixed ansatz of the wave functions (7) the charge density consists of a Fourier and a multipole contribution

$$\rho(\mathbf{r}) =: \sum_{\mathbf{K}_\parallel} \rho_{\mathbf{K}_\parallel}(z) e^{i\mathbf{K}_\parallel \cdot \mathbf{r}_\parallel} + \sum_{l,m} \rho_{lm}(r) Y_{lm}(\mathbf{r}_0), \quad \mathbf{r} \in \Omega, \tag{42}$$

with $\rho_{lm}(r \geqslant r_{\mathrm{MT}}) = \partial_r \rho_{lm}(r \geqslant r_{\mathrm{MT}}) = 0$. (In the vacuum layer $\rho_{lm} \equiv 0$.) While the first sum is finite, the second is not and therefore needs to be truncated in numerical calculations. Below, a maximum value of $l = 8$ is used. Except for the energy integration discussed above, the calculation of these components is straightforward but lengthy and is therefore not given here. For details, see Ref. 42.

Given the charge density, the effective potential is calculated according to the Hohenberg-Kohn-Sham formalism[1,2] as a sum of the electrostatic Potential V_c of the electrons and nuclei and the exchange-correlation potential V_{xc}, where the latter is approximated by a local function of ρ suggested by Gunnarsson and Lundqvist[43]:

$$V_{\mathrm{eff}}(\mathbf{r}) = V_c(\mathbf{r}) + V_{\mathrm{xc}}[\rho(\mathbf{r})]. \tag{43}$$

However, for reasons of numerical stability of the self-consistency procedure, the calculated charge density first has to be restricted according to Eq. (1). This is necessary in order to prevent charge transfers over unlimited distances which may generate arbitrary high fluctuations of the electrostatic potential[44] in the course of the self-consistency procedure.

Because V_c is linear in ρ and V_{xc} is local by assumption it is possible to calculate the potential contributions of each single layer separately using standard techniques[15] and sum them up afterwards. This leads to a more flexible and distinct way of organizing the computation. Given the single layer effective potentials $V_{\mathrm{sl}}^{(k)}$, the total potential within the nth layer is then written as

$$V_{\mathrm{eff}}^{(n)}(\mathbf{r}) = V_{\mathrm{sl}}^{(n)}(\mathbf{r}) + \sum_{k \neq n} V_{\mathrm{sl}}^{(k)}(\mathbf{O}^{(n)} - \mathbf{O}^{(k)} + \mathbf{r}), \quad \mathbf{r} \in \Omega^{(n)}. \tag{44}$$

The electrostatic parts of the single layer potentials are fixed by the condition $V_c^{(n)}(z \to \infty) := 0$. Now, since the contribution of the exchange-correlation potential of the second term is zero within the nth layer, this term is a solution of a homogenous Poisson equation. Thus, for $\mathbf{r} \in \Omega^{(n)}$, it can be represented as

TABLE I. Valence charge distribution over individual layers in electrons.

	$q_{\mathrm{val}}^{(0)}$	$q_{\mathrm{val}}^{(1)}$	$q_{\mathrm{val}}^{(0)} + q_{\mathrm{val}}^{(1)}$	$q_{\mathrm{val}}^{(2)}$
Al(001)	0.360	2.630	2.990	2.974
Al(111)	0.252	2.744	2.996	3.060

$$\sum_{\mathbf{K}_\parallel} e^{i\mathbf{K}_\parallel \cdot \mathbf{r}_\parallel} (e^{+|K_\parallel| z} \omega_{L\mathbf{K}_\parallel}^{(n)} + e^{-|K_\parallel| z} \omega_{R\mathbf{K}_\parallel}^{(n)}) + E^{(n)} z + D^{(n)}, \tag{45}$$

with constants $\omega_{X\mathbf{K}_\parallel}^{(n)}$, $E^{(n)}$, and $D^{(n)}$. What remains is to calculate these constants from the electrostatic part of the single layer potentials at their layer boundaries $V_{\mathrm{sl}}^{(k \neq n)}(z_X)$, which is a straightforward task. Again, the details of computation can be found in Ref. 42. Here, the infinite number of bulk layers with identical charge density [according to Eq. (1)] contribute as a geometric series which is convergent because of their neutrality (41). However, due to Friedel oscillations, the individually treated surface layers need not to be completely neutral. Since there is no compensating net charge within the (by assumption neutral) bulk layers, each lack of neutrality of the surface layers as a whole would cause a small, but in the end unlimited linear increase of the potential for $n \to \infty$ or $z \to -\infty$, respectively. In a real crystal, an unlimited increase of the potential would be prevented by small compensating charges within the bulk. In our case, we assume these compensating bulk charges as being all concentrated at the boundary between bulk and surface layers, so that the bulk layers remain neutral. This assumption leaves the potential of the surface layers untouched and removes just the bothering linear increasing term of the bulk potential.

The redistribution of the compensating bulk charges causes some shift of the bulk potential which actually affects the work function. The error made can be estimated by looking at the total charge of the surface layers as a whole which has to be compensated by these bulk charges. A value which is too high indicates that more surface layers need to be included. In our case (see Table I) this total charge is obviously small enough to be neglected in the calculation of the bulk potential or the work function, respectively.

The Kohn-Sham equations[2] were considered to be self-consistent when the potential matrix elements of two successive iterations have a relative difference of less than 10^{-8}. This quantity also demonstrates the numerical stability of the entire procedure.

Remarks on the total energy and the surface energy. According to the LDA formalism, the following expression for the total energy of the whole crystal can be derived:

$$E_0 = \sum_i E_i \Theta(E_F - E_i) - \frac{1}{2} \int \rho(\mathbf{r}) V_c(\mathbf{r}) d^3\mathbf{r} + \int \{E_{\mathrm{xc}}[\rho(\mathbf{r})] - V_{\mathrm{xc}}[\rho(\mathbf{r})]\} \rho(\mathbf{r})\, d^3\mathbf{r}, \tag{46}$$

which allows an easy separation of the surface-specific part of the total energy from the bulk part. Here, the sum on the right hand side runs over all occupied one particle states, i.e., it comprises an integration over the continuum of bulk states

and a sum over the discrete surface states. As usual, E_{xc} stands for the exchange-correlation energy according to Hedin and Lundqvist and

$$V_{xc}=E_{xc}+\rho\,\frac{\delta E_{xc}}{\delta\rho}. \tag{47}$$

The surface-specific part of the total energy is then given by the above expression with the sum restricted to the discrete surface states and the spatial integrals restricted to the region of the surface layers. All these restricted terms are finite.

From this we obtain the surface energy as the difference between the total energy of the surface layers and the total energy of the same number of bulk layers. This is also the starting point for the calculation of forces or surface reconstructions. We have not carried out explicit calculations of the surface energy so far, but we think that the problems to cope with are similar to those encountered with the calculation of the charge density, so that the integration methods described there are also applicable to Eq. (46).

IV. RESULTS FOR Al(001) AND Al(111)

As a first application the (001) and (111) surfaces of aluminum were calculated self-consistently. To simplify the potential calculation, the higher multipole moments ($l\geqslant 1$) of the potential within the MT spheres were neglected in this first approach. (Nevertheless, the multipole components of the charge density were still included up to $l=8$.) Outside the MT spheres, however, the potential was still fully taken into account (warped-muffin-tin approximation). As the MT radius of our layer geometry is smaller than in the bulk case, the error was expected to be tolerable. It should be noted, that there is no other reason than convenience for this simplification. In particular, it is one of the advantages of the SAPW method to allow an immediate inclusion of the multipole contributions, once they are calculated.[36] Because of the high density of almost free electrons in aluminum the influence of the surface is screened within a short distance.[18] Hence, it seemed reasonable to treat only the first layer as individual surface layer and class all other layers as belonging to the bulk, thus $N_b=2$. So, the numerical effort was essentially determined by two linear systems (13) of rank 250 and one linear system (15) for the vacuum of rank 190, to be solved for each value of $\mathbf{k}_{\|}$ and E. Except for the calculation of the charge density which required about 30% of the total computer time, all other equations are ranked much lower, so that their numerical expense was negligible. Therefore, the numerical effort is fairly small, especially with respect to the precision achieved.

A. Charge density

Figures 4 and 5 show the self-consistent valence charge density of the Al(001) and Al(111) surface, respectively, where the first two layers are depicted together with the infinitely remote bulk layer which is separated by a dashed line. Here, the charge density of the second layer is shown as calculated from the asymptotically correct wave functions, that is before it is replaced by the density of the bulk layer according to Eq. (1). Though the second layer is not self-consistent in the original sense, it bears physical relevance as it is a correct solution for a potential which differs only slightly from a self-consistent one. In particular, the obvious similarity of this layer to the bulk layer exhibits the strong screening of the perturbations induced by the surface. This also applies to the long range Friedel oscillations which are heavily suppressed as a consequence of the high free electron density.[18] Hence, the consideration of only one individual surface layer seems justified *a posteriori*.

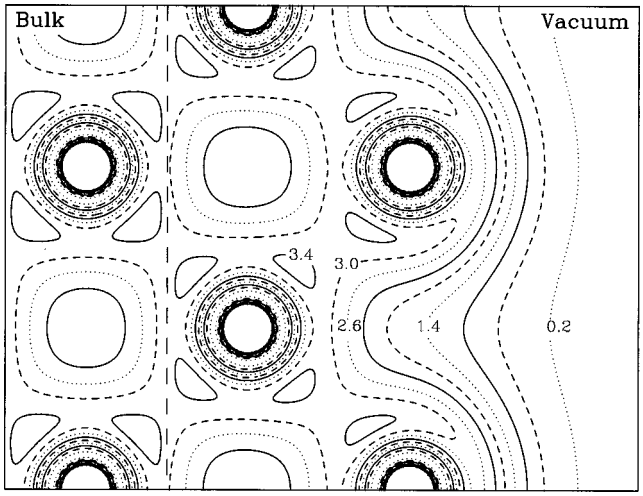

FIG. 4. Valence charge density of the Al(001) surface. Increasing contour lines are cyclically marked in the order dotted, dashed, solid and differ by 0.4 electrons per bulk unit cell.

Considerable charge transfers are essentially limited to the right side of the first layer. Analogously to the uniform background model[17,18] a surface barrier is established as some charges are leaking out into the vacuum region. The distribution of the valence charges over the individual layers is shown in Table I. The good screening properties of Al are demonstrated again, as the sum of the charges within the first layer and the vacuum is almost equal to the bulk value of three electrons. The slightly greater deviation in the second layer is probably due to its lack of self-consistency.

Figure 4 is in very good agreement with the LAPW results of Krakauer *et al.*[11] obtained for a nine-layer slab. The corresponding results of Inglesfield and Benesh,[31] on the

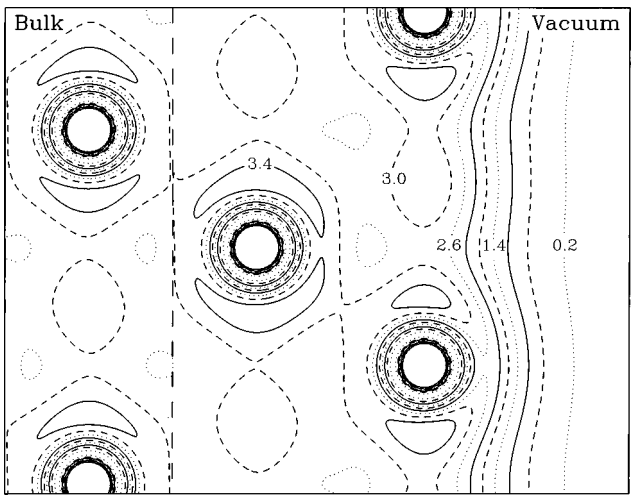

FIG. 5. Valence charge density of the Al(111) surface. Same units as in Fig. 4.

other hand obtained for a semi-infinite geometry by means of the embedded-potential method show some deviations which are probably due to restrictions imposed on parts of their potential.

In case of Al(111) the charge density obtained by other authors[7,12,45,46] differ slightly from Fig. 5, as they do among one another. This is partly due to the lack of symmetry of the ansatz functions, which are subject only to the two-dimensional planar symmetry, while inside the bulk the actual symmetry gradually becomes fcc. In the course of the self-consistency procedure the cubic symmetry of the bulk layers becomes therefore a little blurred. This is only a numerical and no physical effect caused by the lack of cubic symmetry of the ansatz functions. But since the charge density is distributed rather uniformly between the ion cores, the relative error is still rather small. In the (001) case the planar symmetry is better adapted to the cubic symmetry, so the effect is less distinct. A conceivable way to avoid this drawback—reserved for future calculations—is to force an explicit cubic symmetrization of the bulk charge density after each self-consistency cycle.

B. Work function

A first test for the quality of the self-consistent charge density is the precision of the calculated work function, given (exactly) by the difference of the asymptotic vacuum level and the Fermi energy[47] $\phi = V_\infty - E_F$. Here, we obtained a value of $\phi = 4.505$ eV for Al(001) and 4.491 eV for Al(111). These results differ from the experimental values of 4.41 eV (001) (Ref. 48) and 4.26 eV (111) (Ref. 49) by 2 and 5 %, respectively, which seems to be quite good—in view of the numerical effort—compared to other relevant calculations summarized, e.g., in Ref. 5.

In both cases the experimental results are overestimated. This can mainly be attributed to the warped-muffin-tin approximation where the neglection of the dipole contribution of the potential increases the charge transfer into the vacuum and therefore the work function. This relation is also demonstrated by the fact that the error is considerably smaller in the Al(001) case, where the MT radius and therefore the region of the potential restriction is smaller than in the Al(111) case (see also, Ref. 16). Thus, it is expected to obtain more accurate values for the work function, even in the framework of the LDA formalism, if the potential is fully taken into account.

C. Surface band structure

The main advantage of considering a semi-infinite medium instead of a slab of finite thickness becomes particularly significant with the calculation of energy resolved quantities such as the band structure, as this model allows a definite distinction between discrete surface states and continuum states. Moreover, since all surface states and resonances are reliably detectable by means of the techniques described above, the surface band structures of Al(001) and Al(111), shown in Figs. 6 and 7, are expected to be complete.

The bands are embedded in the projected band structure which is depicted as vertical lines indicating the energy intervals of the contiuum states. The surface resonances within the energy continuum are distinguished according to their sharpness by different symbols. Figure 8 gives an idea of the relation between the marking symbols and the sharpness of the resonance peaks. To avoid confusions, only clear peaks are marked.

The band structures agree well with the dispersion curves experimentally obtained so far: Al(001) $\bar{\Delta}$, $\bar{\Sigma}$: Refs. 50 and 52, Al(111) $\bar{\Sigma}$: Ref. 53, and around Al(111) $\bar{K}$: Ref. 57. Moreover, our results fundamentally confirm the theoretical band structures of Heinrichsmeier *et al.*[5] which are extracted from elaborated pseudopotential calculations for slabs consisting of 25 and 39 layers, respectively. The only differences of their results to ours, worth mentioning, are the missing continuation along the (001) $\bar{\Delta}$ direction of the surface state at $\bar{X} - 4.48$ eV below E_F which was also found in Ref.

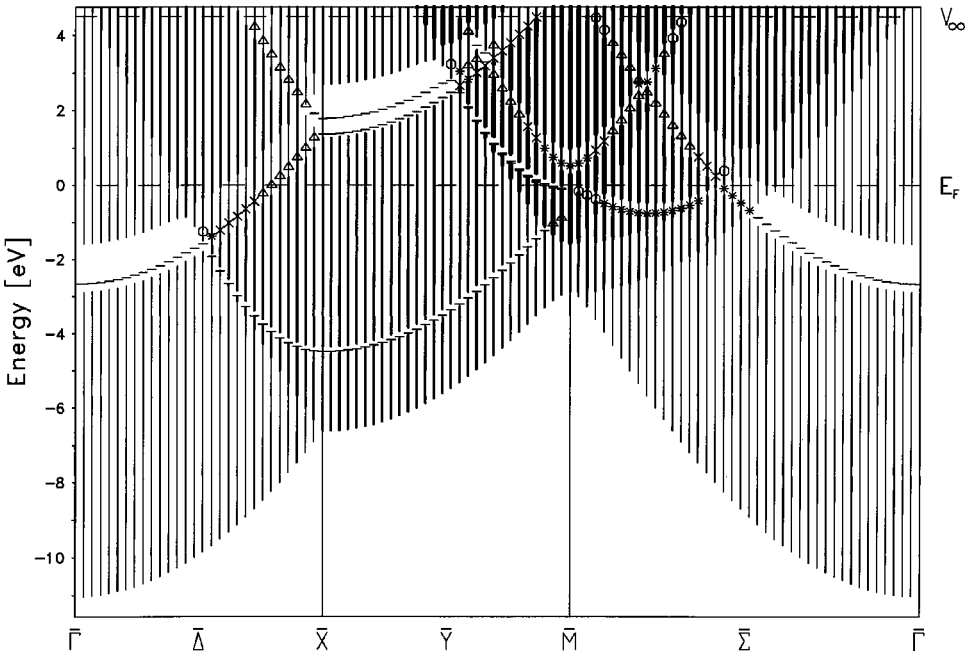

FIG. 6. Surface band structure and projected band structure of Al(001). Surface states are marked with dashes, resonances according to their sharpness with $*$, $\times$, Δ, and $\bigcirc$, indicating the value of $\lambda_{\min}$ from Eq. (36) being less than 0.0025, 0.01, 0.04, or 0.09, respectively. The thickness of the lines of the projected band structure indicates the value of σ_p, i.e., the number of independent solutions.

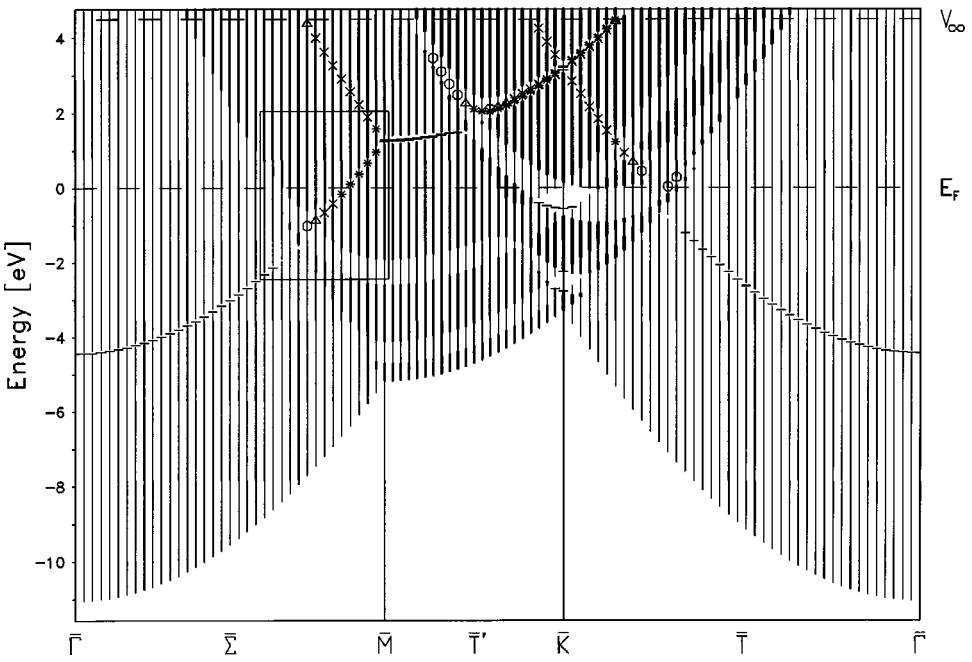

FIG. 7. Surface band structure and projected band structure of Al(111). Symbols as defined in Fig. 6.

24 and partly in Ref. 55, a surplus resonance band along the (111)-X' direction about 0.4 eV above the lower valence band edge, neither reported by other authors, and finally the pair of surface states crossing the Fermi energy on the (001)-Y direction just before the M point which was regarded only as a single state by these authors. In the present work the double nature of this last-mentioned state is clearly revealed. For the Al(001) surface the non-self-consistent results of Wachutka[24] obtained by means of an earlier version of our method exhibit perfect qualitative agreement. The self-consistent Al(111) band structure of Benesh and Liyanage[45] on the other hand, also obtained for a semi-infinite crystal agree on the dispersion of the surface states but differ in the dispersion of several resonances.

Other surface band structures published so far are less complete than those mentioned above. They are discussed in the above mentioned works.

In Fig. 8 the LDOS of the surface layer is depicted as a function of E and $\mathbf{k}_{\parallel}$. This figure clearly shows the transition of the surface states at M into two sharp resonances the lower of which gets wider and finally ''decays.'' On the other hand the surface state coming from the bottom right disappears without leaving any trace in the LDOS. This is due to the fact that this state—lying on an imaginary loop of the complex band structure—spreads into the bulk while getting closer to the band edges. Hence the localization of the wave function and therefore the LDOS decreases and finally vanishes. In contrast to this, the first-mentioned surface states merge with a bulk band of other symmetry than the complex loop, so there is no spreading and rapid hybridization is prevented. These two extreme examples exhibit the principal mechanisms determining the decay behavior of surface states merging with the bulk continuum.

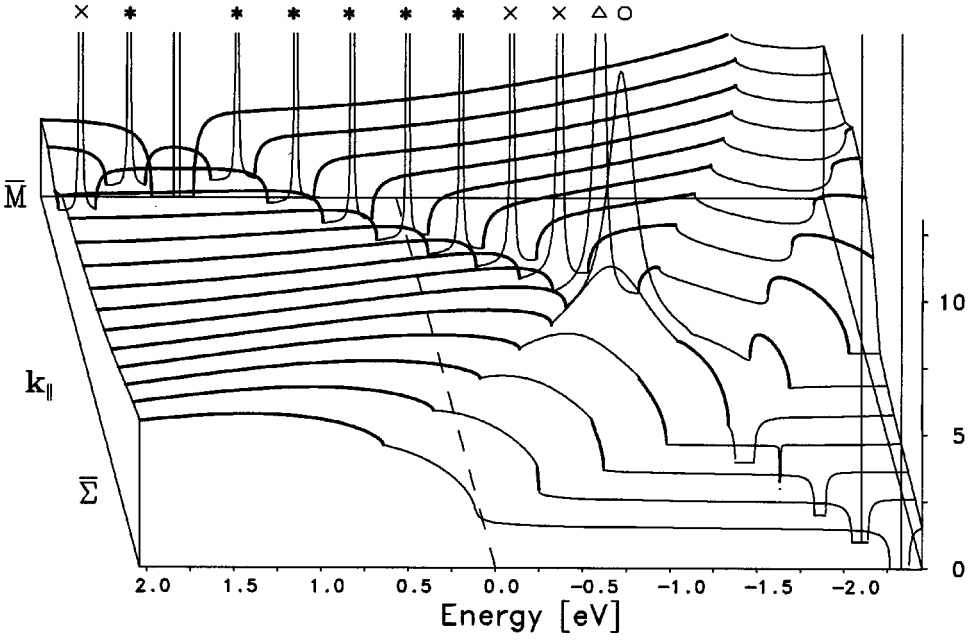

FIG. 8. $\mathbf{k}_{\parallel}$-resolved surface density of states $N^{(1)}(\mathbf{k}_{\parallel},E)$ of the framed area in Fig. 7 in atomic units. The lines correspond to the same $\mathbf{k}_{\parallel}$ vectors as the lines in Fig. 7. Symbols also as defined therein.

TABLE II. Comparison of the surface state energies of Al(001) at the high-symmetry points with experimental and other theoretical works. Energies are given in eV with respect to E_F. The values marked with ~ are taken from depicted graphs.

$\mathbf{k}_\parallel$	This work	Expt.[a]	Ref. 31[b]	24[c]	11[d]	5[e]	55[f]	3[g]
$\bar{\Gamma}$	−2.67	−2.75	−2.65	~−2.6	~−2.9	−2.67	−2.81	−2.73
$\bar{X}$	−4.48	−4.54	−4.61	~−4.6		−4.55	−4.63	−4.71
	1.37	1.5		1.63	~1.1	1.36	~1.3	1.65
	1.79			1.72	~1.8	1.81	~1.9	1.98

[a]Refs. 50,51,52,53,54.
[b]Embedded potential, semi-infinite crystal.
[c]ABCM, semi-infinite crystal.
[d]LAPW, 9 layers.
[e]Pseudopotential, 25 layers.
[f]Pseudopotential, 9 layers.
[g]Pseudopotential, 13–39 layers.

Figure 8 also resolves the debate about some experimental observations concerning the structure of a surface resonance. Initially, Hansson and Flodström[52] concluded from their angle-resolved photoemission experiments the existence of a surface resonance within this area with a dispersion opposite to that in Fig. 8. This interpretation, however, was questioned by Grepstad and Slagsvold[56] and later by Hofmann and Kambe[57] who detected some properties difficult to reconcile with surface resonances. Therefore, they interpreted this structure as caused by bulk transitions. In spite of that Grepstad and Slagsvold[56] still observed some indications for surface resonances within the area in question. A theoretical interpretation of these results was given by Heinrichsmeier *et al.*[5] who attributed the structure observed in Ref. 52 to a so called ''broad resonance'' that is a continuum of bulk states with increased amplitude near the surface. In addition they found a true sharp resonance of opposite dispersion within the same area explaining the observations of the latter authors as well. This interpretation is now strongly supported by Fig. 8 which clearly exhibits the different character of the sharp resonance and a broad increase of the LDOS with opposite dispersion.

In Tables II and III the energies of the surface states at high symmetry points are listed and compared with both the experimental and the theoretical results of other authors. The comparison shows a good agreement with experiment within a range of 0.1 eV. Besides that, the energies of the surface states which are not observed experimentally yet, precisely confirm the values predicted by Heinrichsmeier *et al.*[5] As is demonstrated again by these tables the main advantage of our method is the completeness and unambiguity of the spectrum which can be achieved with little numerical effort.

V. SUMMARY

We have developed an effective method for calculating the self-consistent electronic structure of realistic crystal sur-

TABLE III. Comparison of the surface state energies of Al(111) at the high-symmetry points with experimental and other theoretical works. Energies are given in eV with respect to E_F.

$\mathbf{k}_\parallel$	This work	Expt.[a]	Ref. 45[b]	7[c]	12[d]	5[e]	46[f]	58[g]
$\bar{\Gamma}$	−4.44	−4.56	−4.58	−4.68		−4.60	−4.49	−4.69
$\bar{M}$	1.24		1.20	1.09		1.11		
	1.28		1.30			1.22		1.29
$\bar{K}$	−2.78	−2.7	−2.71	−2.81		−2.78		
	−2.25		−2.50	−2.58	−2.4	−2.57	−2.04	−2.64
	−0.55	−0.7	−0.60	−0.65	−0.58	−0.69	−0.95	−0.67
	3.14					3.08		
	3.21					3.19		3.52
	3.25					3.21		

[a]Refs. 56,57,53.
[b]Embedded potential, semi-infinite crystal.
[c]LCGO, 18 layers.
[d]LAPW, 9 layers.
[e]Pseudopotential, 36 layers.
[f]Pseudopotential, 12 layers.
[g]Pseudopotential, 13–33 layers.

faces or general interfaces within the *ab initio* LDA scheme. The underlying model of a semi-infinite medium allows an *exact* distinction between interface and bulk effects. A second advantage is that the numerical effort is determined only by the small number of interface layers differing considerably from a bulk layer and that it increases only *linearly* with that number. Because of this linear behavior the method is especially suited for the investigation of interfaces of materials with bad screening properties such as semiconductors or insulators which require a greater number of individually treated interface layers. The method is based on wave-function matching as proposed by Appelbaum and Hamann[19] but in contrast to these authors the propagation matrix technique[21] is not used as it turned out to be numerically unstable. Instead, as a generalization of the ideas of Wachutka,[24] we used a technique essentially based on the solution of homogeneous underdetermined linear equations which makes those numerical problems disappear completely. Within this scheme interface states and resonances are uniquely identifiable and reliably localizable by looking at the eigenvalues of a ''mismatch matrix,'' thus the interface band structures obtained are expected to be complete.

First self-consistent results are obtained for the (001) and (111) surfaces of Al. Because of the good screening properties of the conduction electrons it turns out to be sufficient to consider only one surface layer as independent from the bulk. Within this configuration the theoretical results are in very good agreement with the experiments.

[1] P. Hohenberg and W. Kohn, Phys. Rev. **136**, B864 (1964).
[2] W. Kohn and L. J. Sham, Phys. Rev. **140**, 1133 (1965).
[3] E. Caruthers, L. Kleinman, and G. P. Alldredge, Phys. Rev. B **8**, 4570 (1973).
[4] M. Schlüter, J. R. Chelikowsky, S. G. Louie, and M. L. Cohen, Phys. Rev. B **12**, 4200 (1975).
[5] M. Heinrichsmeier, A. F. Fleszar, and A. G. Eguiluz, Surf. Sci. **285**, 129 (1993).
[6] D. S. Wang and A. J. Freeman, Phys. Rev. B **19**, 793 (1979).
[7] K. Mednick and L. Kleinman, Phys. Rev. B **22**, 5768 (1980).
[8] J. A. Appelbaum and D. R. Hamann, Solid State Commun. **27**, 881 (1978).
[9] H. Krakauer, M. Posternak, and A. J. Freeman, Phys. Rev. Lett. **41**, 1072 (1978).
[10] O. Jepsen, J. Madsen, and O. K. Andersen, Phys. Rev. B **18**, 605 (1978).
[11] H. Krakauer, M. Posternak, A. J. Freeman, and D. D. Koelling, Phys. Rev. B **23**, 3859 (1981).
[12] D. S. Wang, A. J. Freeman, H. Krakauer, and M. Posternak, Phys. Rev. B **23**, 1685 (1981).
[13] E. Wimmer, H. Krakauer, M. Weinert, and A. J. Freeman, Phys. Rev. B **24**, 864 (1981).
[14] E. Wimmer, M. Weinert, A. J. Freeman, and H. Krakauer, Phys. Rev. B **24**, 2292 (1981).
[15] H. Bross and M. Kauzmann, Phys. Rev. B **51**, 17 135 (1995).
[16] M. Kauzmann, Ph.D. thesis, Munich University, 1993.
[17] N. D. Lang and W. Kohn, Phys. Rev. B **1**, 4555 (1970).
[18] N. D. Lang and W. Kohn, Phys. Rev. B **3**, 1215 (1971).
[19] J. A. Appelbaum and D. R. Hamann, Phys. Rev. B **6**, 2166 (1972).
[20] J. A. Appelbaum, G. A. Baraff, and D. R. Hamann, Phys. Rev. B **11**, 3822 (1975).
[21] P. M. Marcus and D. W. Jepsen, Phys. Rev. Lett. **20**, 925 (1968).
[22] D. W. Jepsen and P. M. Marcus, in *Computational Methods in Band Theory*, edited by P. M. Marcus, J. F. Janak, and A. R. Williams (Plenum, New York, 1971).
[23] G. Wachutka, Ann. Phys. (N.Y.) **187**, 269 (1988); **187**, 314 (1988).
[24] G. Wachutka, Phys. Rev. B **34**, 8512 (1986).
[25] G. Wachutka, Diploma thesis, Munich University, 1978.
[26] N. A. W. Holzwarth and M. J. G. Lee, Phys. Rev. B **18**, 5350 (1978).
[27] K. Kambe, Z. Naturforsch. A **22**, 322 (1967); **22**, 422 (1967).
[28] G. A. Benesh and J. E. Inglesfield, J. Phys. C **17**, 1595 (1984).
[29] P. Krüger and J. Pollmann, Phys. Rev. B **38**, 10 578 (1988).
[30] H. L. Skriver and N. M. Rosengaard, Phys. Rev. B **46**, 7157 (1992).
[31] J. E. Ingelsfield and G. A. Benesh, Phys. Rev. B **37**, 6682 (1988).
[32] V. Heine, Proc. Phys. Soc. London **81**, 300 (1963).
[33] E. G. McRae, Surf. Sci. **11**, 479 (1968).
[34] D. W. Jepsen, Phys. Rev. B **22**, 5701 (1980).
[35] P. M. Morse and H. Feshbach, *Methods of Theoretical Physics* (McGraw-Hill, New York, 1954), Vol. 1, p. 677ff.
[36] G. Fehrenbach and H. Bross, Phys. Rev. B **48**, 17 703 (1993).
[37] C. de Boor, *A Practical Guide to Splines* (Springer, Berlin, 1978).
[38] D. J. Chadi and M. L. Cohen, Phys. Rev. B **8**, 5747 (1973).
[39] H. Bross (unpublished).
[40] S. L. Cunningham, Phys. Rev. B **10**, 4988 (1974).
[41] J. E. Inglesfield, Surf. Sci. **76**, 355 (1978).
[42] W. Hummel, Ph.D. thesis, Munich University, 1995.
[43] O. Gunnarsson and B. I. Lundqvist, Phys. Rev. B **13**, 4274 (1976).
[44] E. Hahn, Ph.D. thesis, Munich University, 1987.
[45] G. A. Benesh and L. S. G. Liyanage, Phys. Rev. B **49**, 17 264 (1994).
[46] J. R. Chelikowsky, M. Schlüter, S. G. Louie, and M. L. Cohen, Solid State Commun. **17**, 1103 (1975).
[47] F. K. Schulte, Z. Phys. B **27**, 303 (1977).
[48] J. K. Grepstad, P. O. Gartland, and B. J. Slagsvold, Surf. Sci. **57**, 348 (1976).
[49] P. O. Gartland, Surf. Sci. **62**, 183 (1977).
[50] P. O. Gartland and B. J. Slagsvold, Solid State Commun. **25**, 489 (1978).
[51] M. Gautier, E. Marteaux, J. P. Duraud, R. Baptist, A. Brenac, and D. Spanjaard, J. Vac. Sci. Technol. A **5**, 550 (1987).
[52] G. V. Hansson and S. A. Flodström, Phys. Rev. B **18**, 1562 (1978).
[53] S. D. Kevan, N. G. Stoffel, and N. V. Smith, Phys. Rev. B **31**, 1788 (1985).
[54] H. J. Levinson, F. Greuter, and E. W. Plummer, Phys. Rev. B **27**, 727 (1983).
[55] E. V. Chulkov and V. M. Silkin, Surf. Sci. **215**, 385 (1989).
[56] J. K. Grepstad and B. J. Slagsvold, Phys. Scr. **25**, 813 (1982).
[57] P. Hofmann and K. Kambe, Phys. Rev. B **30**, 3028 (1984).
[58] E. Caruthers, L. Kleinman, and G. P. Alldredge, Phys. Rev. B **9**, 3330 (1974).